DOI: 10.31401/WS.2020.proc.17

Registration of Neutrons with a Single Detector Liulin Type Spectrometer

Dachev[1] T., Tomov[1] B., Matviichuk[1] Y., Dimitrov[1] P., Semkova[1] J., Jordanova[1] M., Bankov[1] N., Ploc[2] O., Litvak[3] M., Tretyakov[3] V., Shurshakov[4] V., Benghin[4] V.

[1]Space Research and Technology Institute, Bulgarian Academy of Sciences, Sofia, Bulgaria
E-mail: tdachev@bas.bg

[2]Nuclear Physics Institute, Check Academy of Sciences, Prague, Czech Republic

[3]Space Research Institute, Russian Academy of Sciences, Moscow, Russia

[4]State Research Center Institute of Biomedical Problems, Russian Academy of Science, Moscow, Russia

Abstract

The analysis of the experimental energy deposition spectra, obtained with a single detector Liulin type spectrometer (SDLTS), reveal that in the high-energy deposition channels of the spectra exist count events that cannot be explained only with the depositions from charged particles. These events are well seen in the spectra from the calibrations with protons and radionuclide neutron sources as well as in the CERN radiation field and aircraft, balloon and spacecraft spectra. If the high-energy deposition events are from protons, their energy must be mainly in the range 1-15 MeV [Simpson, 1983]. The paper reviews all mentioned above spectra and concludes that these events could be explained with the registration of neutrons in the energy range 1-100 MeV.

Introduction

Onboard space vehicle radiation fields are composed primary of galactic cosmic rays (GCR) as well as of secondary particles, created during the nuclear interactions of the primary radiation with the matter of the spacecraft and the detector. As far as the contribution of these secondary particles to the exposure level is concerned, relatively the most important is that of neutrons. [Spurny et al., 2007].

Around the International space station (ISS), a neutron emission is produced due to the interactions of energetic charged particles of the magnetosphere with the matter of the station itself [Sevast'yanov et al., 1997]. These local neutron fluxes are present around the station. They vary along the station orbit due to the irregularity of the flux of charged particles. At balloon and aircraft altitudes, neutrons are produced also by the interaction of the primary GCR protons with the atmosphere.

Instruments description

Fig. 1 presents a generalized block diagram of a single detector Liulin type spectrometer (SDLTS) [Dachev et al., 2015]. The SDLTS usually contains one semiconductor detector, one charge-sensitive preamplifier, a fast 256-channel analogue-to-digital converter (ADC), a discriminator, a real time clock, two or more microcontrollers and a flash memory. The different modifications of Liulin spectrometers use additional modules such as visible and UV sensitive photodiodes, a temperature sensor, a Global Positioning System (GPS) module with an antenna and receiver, LED or LCD display, multimedia card (MMC) or SD card.

The measurement cycles of the SDLTS instruments is between 10 and 600 s. During this time, one energy deposition spectrum (EDS) from the cosmic ionizing radiation is accumulated and further used for the calculation of the absorbed dose and flux in the silicon detector [Dachev, 2009]. A system international (SI) determination of the dose is used to calculate the absorbed dose in the silicon detector. The dose in SI is the energy in Joules deposited in one kilogram of a matter. The following equation relates the dose to energy loss and detector mass:

$$D = K * \sum_{1}^{256}(Ei * Ai)/MD \qquad (1)$$

where *MD* is the mass of the detector (in kg), *Ei* is the energy loss (in J) in the channel *i*, *Ai* is the number of events in it, and *K* is a coefficient. Dachev et al [2017] have already published a more comprehensive descriptions of the dose calculation procedures and the radiation sources selection procedures. Therefore, we will skip those details here.

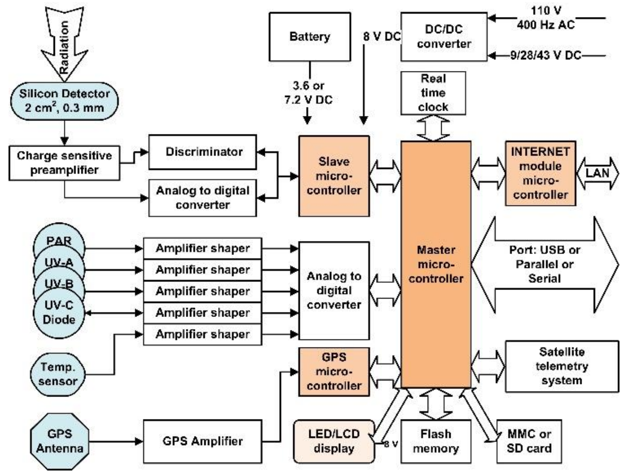

Fig. 1. Generalized block diagram of single detector Liulin type spectrometer (SDLTS).

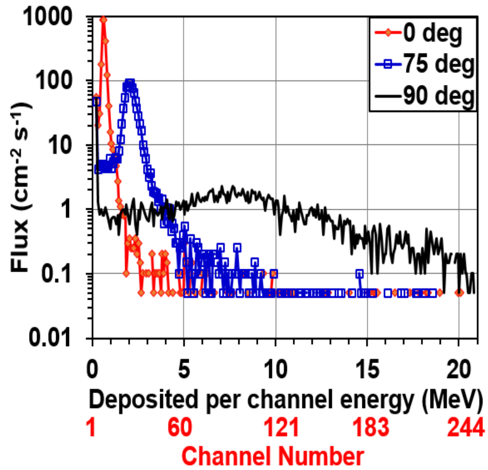

Fig. 2 Energy deposition spectra obtained during the calibrations with 32 MeV proton flux.

Methodic of neutron flux and dose recognition in the Liulin data

Recognition of the neutron events in the EDS during calibration

Fig. 2 presents 3 energy deposition spectra obtained in the end of 1999 during the calibration of the mobile dosimetry unit number 1 (MDU-1) of Liulin-E094 instrument with a proton beam at the cyclotron facility in the Universite Catholique de Louvain, Louvain-la-Neuve, Belgium [Dachev et al., 2002]. The 65 MeV protons pencil beam delivered by the accelerator passes through collimators, 14 mm graphite absorber and 1 mm thick scintillator.

The final proton beam was with 3-cm^2 area and 32 MeV energy. The detector of the MDU was irradiated from three different incidence angles of 0°, 75° and 90° against the detector's plane. The 0° EDS (red curve) maximum is at about 1 MeV deposited energy, which is the smallest one because in this case the protons cross the detector with a minimal path length. The maximum of the 75° spectrum is seen at 2 MeV energy deposition. In the 0° and 75° spectra in the channels numbers greater than 120 single events are observed. Low energy protons or secondary neutrons could produce them, while interacting with the surrounding experimental matter including the Silicon of the detector. The same mechanism is observed in the South Atlantic Anomaly (SAA). The high-energy depositions registered in this region are produced by the long path protons and neutrons interactions with the detector. The 90° spectrum is spread over the whole energy spectra of the EDS because both the primary and the secondary particles pass the longest side (20 mm) of the detector and produce very high-energy depositions.

To investigate more precisely the neutron sensitivity of the Si (silicium) detector in the Liulin instruments, Professor Frantisek Spurny performed series of calibrations with different neutron sources [Spurny, 2005].

Fig. 3 presents some of the results together with experimental GCR spectra obtained at aircraft and at the ISS. Seven different averaged spectra are plotted. The shortest EDS are those obtained from the ^{137}Cs gamma and the AmF radionuclide sources with an average energy of the neutrons of 1.5 MeV. The 2.1 MeV ^{252}Cf spectrum extends up to about 3.7 MeV. The average 4.2 MeV AmBe spectrum goes up to 8 MeV deposited energy. The longest neutron source spectrum is the CERN 50 MeV spectrum, which covers the entire energy range. It is received behind a concrete shield [Mitaroff and Silari, 2002]. The region below 2 MeV is increased because of the low energy transfer (LET) - muon particles.

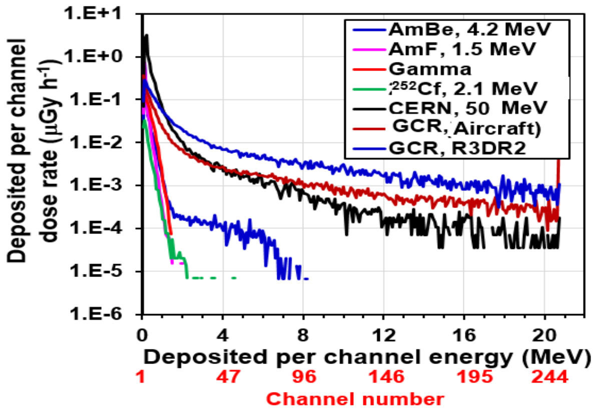

Fig. 3. Neutron sources spectra comparison.

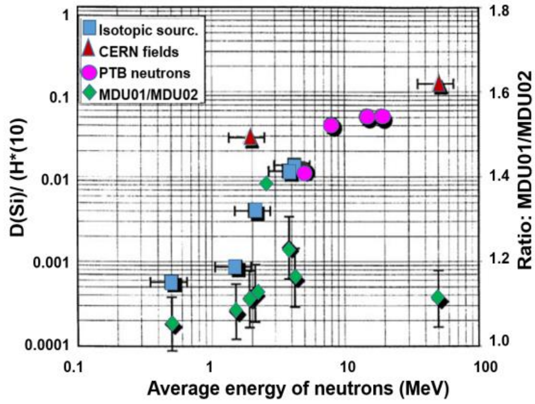

Fig. 4 Relative responses of MDUs in terms of ambient dose equivalent (D(Si)/H∗(10).

The first conclusion from Fig. 3 is that the length of the neutron spectrum depends on the average energy of the neutrons in it. The second conclusion is that the spectrum above 1-1.5 MeV deposited energy is generated by high LET particles with a predominance of neutrons. This is confirmed from the similarities with the CERN, GCR aircraft and spacecraft spectra.

Fig 4 summarizes the results of the calibrations obtained by Prof. Spurny with two MDU units in the following three neutron fields: Isotopic neutron sources, CEC–EC high-energy reference fields [Mitaroff and Silari, 2002] and PTB Braunschweig neutrons reference beams [Guldbakke et al., 1994]. To increase the response toward neutrons, an additional polyethylene layer with a thickness of 1 mm was inserted before the MDU01 detector.

The total values of the doses in Si in the MDUs were calculated by means of Eq. (1). It was consider that the part of the spectrum above 1 MeV deposited energy is populated by neutrons and neutron-like particles that is why the dose rate of this part is denoted as ambient dose equivalents *H*(10)*.

The following conclusions could be drawn from Fig. 4 [Spurny, 2005]:

1. The additional polyethylene layer actually increases the response (see ratio MDU01/MDU02 in Fig. 4) maximum about 20% for the AmBe and PuBe sources. Perhaps this is due to the direct contact of the epoxy resin layer with the Si detector. When the neutrons reach the MDU02 recoil protons are created.

2. The ratio *D(Si) /H*(10)* increases very rapidly with neutron energy. This ratio is 200 times higher for the CERN 50 MeV field behind a concrete shield (most right red triangle point) compared with the AmLi neutron source (the most left blue quadrat point). The latter is the field with the lowest average energy of 1.5 MeV. Such behavior is expected, because the both the total neutron interaction cross section and as well as the energy transferred to high LET secondary charged particles increase substantially with neutron energy [ICRU, 2000].

The last, known yet tests of SDLTS in ^{252}Cf neutron field were performed by [Straume et al. 2016] prior to the NASA high-altitude balloon flight, the RaD-X mission [Mertens, 2016., Mertens et al. 2016]. Four radiation dosimeters were on RaD-X board: a Far West HAWK tissue equivalent proportional counter (TEPC version 3) (https://www.fwt.com/detector/fw-ad1ds.htm), a Teledyne dosimeter (UDOS001), a Liulin dosimeter (MDU 6SA1), and a RaySure dosimeter (version 3b). For ^{252}Cf neutron radiation, Liulin provides absorbed dose rate of 3.14 ± 0.28 µGy h^{-1}in ICRU (International Commission on Radiation Units and Measurements) soft tissue. This is lower than the observed with the TEPC dose of 5.09 ± µGy h^{-1}, measured on the same date.

Recognition of the neutron events in the EDS at aircraft, balloon and spacecraft

Fig. 3 reveals that the shapes of the average CERN, aircraft and spacecraft spectra are very similar. The aircraft spectrum averages long-term data obtained between 2001 and 2005 by colleagues from Nuclear Physics Institute, Academy of Sciences of the Czech Republic [Spurny et al., 2007]. The ISS GCR spectrum is obtained between November 2014 and January 2016 by radiation risk radiometer-dosimeter (R3D)-R2 (R3DR2) instrument [Dachev et al. 2017]. The shapes of the GCR spectra curves at aircraft and spacecraft show a part with a high slope in the low energy deposition region and a smaller slope part, with an almost linear form in the energy deposition part above channel number 47. We consider that the high slope parts of the aircraft and spacecraft spectra contain mainly high-energy charged particles, while the small slope parts are build up mainly by neutrons, sporadic low energy protons with a long path in the detector and rare hi Z energy (HZE) particles. The paper "A comparison of the neutron dose measurements completed by the Bulgarian and Russian instruments outside the Zvezda module of the ISS" (Dachev et al. 2020), in this issue, more comprehensively develop these ideas.

Fig. 5 and 6 visualize the single energy deposition events in the SDLTS instruments spectra at aircraft, balloon and spacecraft that are interpreted as registrations of neutron particles. These events are illustrated in Fig. 5a, 5b, 5d and Fig. 6a with single points above the dashed lines at 15th or 48th channels in the GCR spectra; at the 148th channel in the inner radiation belt (IRB) and solar energetic particle (SEP) spectra and at the 24th channel in the outer radiation belt (ORB) spectra.

Fig. 5a presents the SDLTS 600 seconds resolution parameters' measurements along the aircraft path from Prague to New York during an Intense Solar Flare, Ground Level Event 60, on April 15th, 2001 [Spurny and Dachev, 2001]. Fig. 5c illustrates how the solar event produced an excess in the 'normal' exposure level due to the galactic component (as given by CARI 6) that was a little more than twice the dose rate in the silicon diode. The apparent effective dose, recalculated based on the CERN calibration, is about 80%, from the event rate.

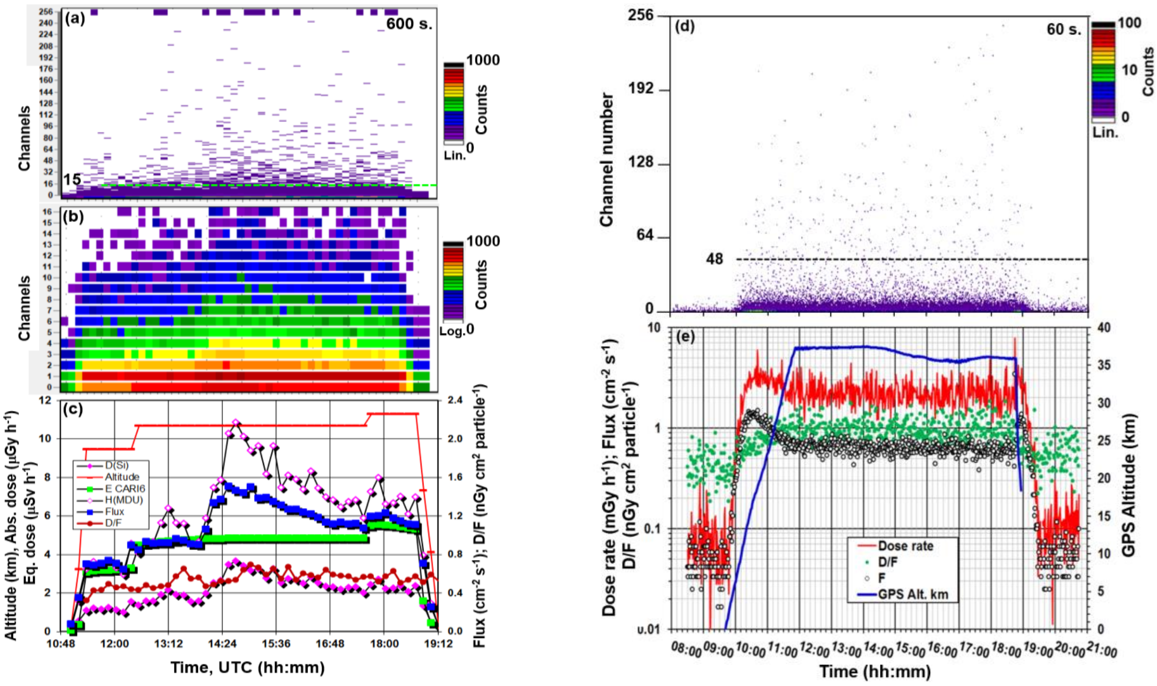

Fig. 5. Fig. 5a: 3D color-coded graphic showing the spectra channels population in the GCR radiation source in the channels range 0-256; Fig. 5b: 3D color-coded graphic showing the spectra channels population in the GCR radiation source in the channels range 0-16; Fig. 5c Analysis of the variations of the: altitude, absorbed and equivalent dose rate, flux and D/F ratio values along the aircraft trajectory on April 15, 2001; Fig. 5d and 5e are similar to the Fig. 5b and Fig. 5c but for the balloon flight.

The counts in all-256 channels of the spectrometer are shown on Fig. 5a. Well seen is that in the channels numbers above 15 or 48 energy deposition events (counts) are registered. Charged particles cannot explain these events. We interpret these events as neutrons. This is confirmed by the fact that these events are not observed at the altitudes below 7 km. The same effect is even better illustrated in Fig. 5d during a balloon flight. The above assumption is also supported and is in line with Friedberg and Copeland publication (2011). The authors demonstrated that the contribution of the neutrons to the mean effective dose rate starts to dominate over the muons and other charged components at a high geographic latitude at 7 km altitude.

The analysis of Fig 5a and 5b reveal that enhanced fluxes and doses are registered in the neutrons channels (Fig. 5a) and in the charged particle channels (Fig. 5b) during the maximum of the solar proton flux at about 14:30 UT. The crossings of the Photzer maximum, seen in Fig. 5d and 5e, does not affect the neutron count rate.

Fig. 6 visualizes the energy deposition events in the R3DR2 instrument data that are interpret as neutron particles registrations. These events are marked in Fig. 6a with blue points above the dashed lines at 48^{th} channel in the GCR spectra; at 148^{th} channel in the IRB and SEP spectra and at 24^{th} channel in the ORB spectra.

Fig. 6a is a 3D presentation of the counts in each channel of the spectrometer from one to 256. The amount of counts is encoded with the color bar at the right-upper corner of the figure. The linear organization of the data in Fig. 6a allows the visualization of the single particles, seen as blue points in the channels of the spectrum. The dotted lines and the numbers near them denoted the upper boundary of the spectra, where the low LET particles are observed. We assume that the parts of the spectra above the dotted lines contain high-energy deposition (high LET) particles, mainly neutrons, long path low energy protons and ions heavier than H^+. As well as protons penetrating trough the side walls of the detector.

Fig. 6b studies what are the absorbed and neutron dose equivalent rates and the dose to flux ratio (D/F) distribution in four typical radiation sources along the 640 spectra of the ISS orbits in May-June 2015. The data from R3DR2 instrument are used. The neutron dose equivalent rate is calculated for each source, using the methodic described in the paper by Dachev et al., "A comparison of the neutron dose measurements completed by the Bulgarian and Russian instruments outside the Zvezda module of the ISS" in this issue. The dashed black line in the bottom of Fig. 6b shows the value of the dose to flux ratio D/F equal to 1-nGy cm^2 $particle^{-1}$.

The first part of measurements numbered from zero to 270 in Fig. 6b shows data obtained on May 5, 2015 between 17:00:07 and 17:46:56 UT. The station crosses a region of a GCR radiation. Fig. 6b illustrates that the absorbed dose rate has a maximum up to about 15 μGy h^{-1}, connected with the passing of the south high latitude region with a maximal L-value of 5.33 [McIlwain, 1961]. The measured neutron dose equivalent rate (black lines and dots) follows, with larger values, the absorbed dose curve (blue). The spectra with numbers larger than 180 are with a smaller absorbed dose rate because of the crossings of the magnetic equatorial region with a minimal value of L=1.02. In the equatorial region, the absorbed dose rate curve shows a minimum with an average value of 0.66 μGy h^{-1}. The equivalent dose rate curve disappears in this region because there are no counts above channel number 48 (Fig. 6a). When all of these channels are empty, the equivalent dose is zero.

The dose to flux ratio in the first 240 measurements (Fig. 6b, red line), has a values close 1-nGy cm^2 $particle^{-1}$ because the GCR source is mainly from high-energy protons. Their energy depositions are relatively small. This is expected from the Haffner's formulae [Haffner, 1967]. A bit smaller D/F values in the equatorial region are generated by the proton spectra with a higher average energy than in the high latitudes.

The geomagnetic shielding, measured by the vertical cutoff rigidity [Smart & Shea, 2005], is the reason for the reducing of the GCR count rates at low L values. At the higher L values the vertical cutoff rigidity decreases and the major amount of the low-energy GCR particles penetrates down to the station's orbit and produces the high latitude maximum.

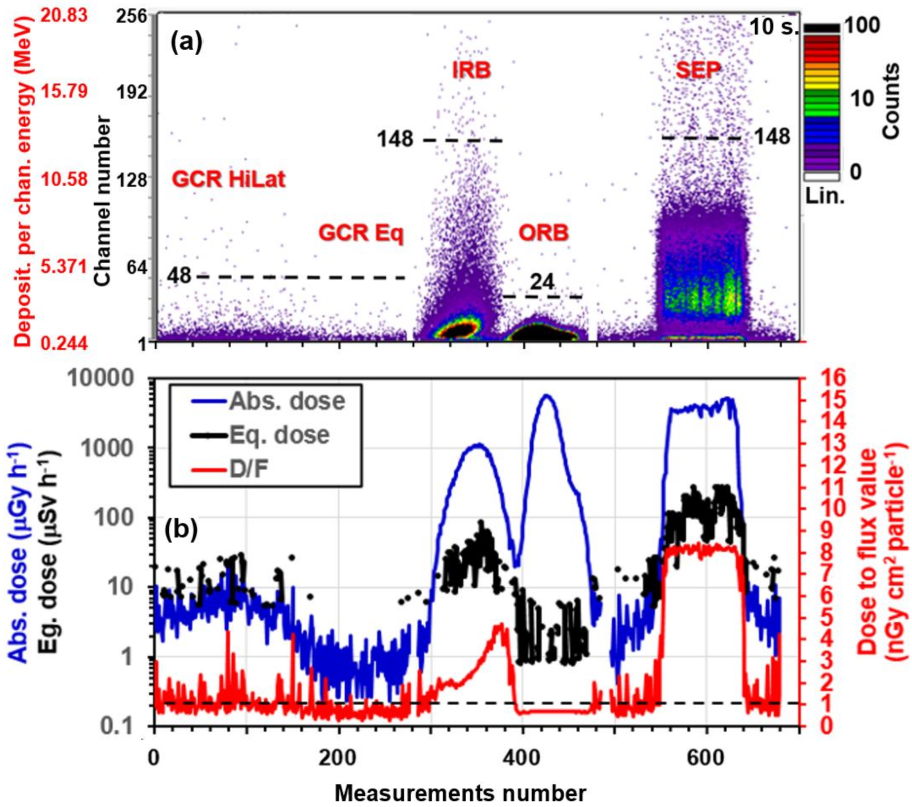

Fig. 6. Fig. 6a: 3D color-coded graphic showing the spectra channels population in different radiation sources. Fig. 6b Analysis of the variations of the absorbed and equivalent dose rate values and D/F ratio along the different radiation sources seen with red labels in Fig. 6a.

The measurements from 280 to 480 (Fig. 6) contain data from the descending ISS orbit, which first crosses the region of the SAA and immediately after that - the outer radiation belt (ORB) region. The absorbed dose rate curve in Fig. 6b shows two maxima. The IRB maximum is smaller than the ORB. The neutron dose equivalent rate generally follows the absorbed dose rate in the region of the IRB maximum. It has about two order of magnitude smaller values. In the region of the ORB maximum the equivalent dose rate curve anti correlates the absorbed dose rate. The behavior of the D/F ratio (red curve) confirms the findings for the dose rates. In the IRB region, the D/F ratio is all above 1-nGy cm^2 particle^{-1} because the protons, with energies 30-400 MeV, deposit higher dose than the protons from the GCR source. The latter are with much higher energies and smaller energy depositions. We calculate the values of the proton energy in the equatorial edge of the SAA maximum and receive an average value of 49 MeV, using the Haffner's formulae [Haffner, 1967]. After crossings of the SAA maximum at coordinates of (44.98ºW, 28.09ºS) in the poleward edge of the SAA maximum, the D/F vales rise up to about 4 nGy cm^2 particle^{-1} showing smaller proton energies of about 30 MeV.

The part of the 3D graphic in Fig. 6a, which represents the SAA maximum confirms the findings above. The spectrum maximum position against the red energy deposition axis in the left part of Fig. 6a is the first with smaller energy depositions per channel, which means a higher proton energy. Further, with the movement of the ISS across the SAA the energy depositions in the maximum rise up to higher value and respectively higher channel number, meaning that the energy of the impinging protons falls down.

The large amount of blue points above the IRB maximum in Fig. 6a is generated mainly by the long path low-energy protons, populating these channels in the same way as the high-energy points in the inclined spectra with 75º and 90º in Fig. 3. We consider that mainly the secondary neutrons generate the counts above the 148th channel.

The analysis of the spectra in the ORB maximum in Fig 6a shows that they are with a single maximum at the low energy depositions as expected from the relativistic electrons. Above the channel 24 there are very small number of counts, probably generated by sporadically GCR protons. All D/F values in the ORB region (Fig. 6b) are smaller than 1-nGy cm^2 particle^{-1}, as expected from the Haffner's formulae [Haffner, 1967].

The SEP maximum (last part of data in Fig. 6) is obtained between 20:02:34 and 20:16:14 UT on 22 June 2015. It is the highest maximum of this SEP event with a maximal dose rate of 5,242-μGy h^{-1} at 20:13:44 UT. The spectra in Fig. 6a shows small maximum in the first channels generated by the GCR particles. Further, there is a broad maximum in channels 30-90, generated by the 7 MeV SEP protons at the detector surface (Dachev et al., 2016).

Conclusions

The purpose of this paper is to demonstrate that a single detector Liulin type spectrometer is able to register neutrons in the energy range 1-100 MeV.

The presented evidences from the calibrations with protons and radionuclide neutron sources as well as from the CERN radiation field and aircraft, balloon and spacecraft spectra confirm that the Liulin type instruments do have the sensitivity to detect neutrons with energies above 1 MeV. The SDLTS is used for a neutron dose equivalent rate calculation, measured with the R3DR instrument on the ISS, and for a comparison with the Russian BTN-NEUTRON instrument data. The results are presented in the paper by Dachev et al., named "A comparison of the neutron dose measurements completed by the Bulgarian and Russian instruments outside the Zvezda module of the ISS" in this issue.

Acknowledgements

This work is supported by: Agreement between RAS and BAS on "Fundamental space research", Contract No. 4000117692/16/NL/NDe Funded by the Government of Bulgaria through an ESA Contract under the PECS (Plan for European Cooperating States), Contract with National Science Fund –Bulgaria on Project N 129 FOR BILATERAL PROJECTS – BULGARIA – RUSSIA 2018 -2019. In IKI-RAS the work is supported by the Russian Science Foundation under grant 19-52-18009. NPI work was funded by the European Structural and Investment Funds under the Operational Program Research, Development and Education (project CRREAT CZ.02.1.01/0.0/0.0/15_003/0000481).

Most of the data used in this paper are part of the "Unified web-based database with Liulin-type instruments", which are available online, free of charge at the following URL: http://esa-pro.space.bas.bg/database. The database was created under the ESA contract mentioned above.

References

Dachev Ts., B. Tomov, Yu. Matviichuk, Pl. Dimitrov, J. Lemaire, Gh. Gregoire, M. Cyamukungu, H. Schmitz, K. Fujitaka, Y. Uchihori, H. Kitamura, G. Reitz, R. Beaujean, V. Petrov, V. Shurshakov, V. Benghin, F. Spurny, (2002), Calibration Results Obtained With Liulin-4 Type Dosimeters. Adv. Space Res. 30, 4, 917-925. http://dx.doi.org/10.1016/S0273-1177(02)00411-8.

Dachev, Ts.P., (2009), Characterization of near Earth radiation environment by Liulin type instruments, Adv. Space Res., 44, 1441-1449. http://dx.doi.org/10.1016/j.asr.2009.08.007

Dachev, T.P., J.V. Semkova, B.T. Tomov, Yu.N. Matviichuk, Pl.G. S. Maltchev, R. Koleva, Pl., Dimitrov, N.G. Bankov, V.V., Shurshakov, V.V., Benghin, E.N., Yarmanova, O.A. Ivanova, D.-P. Häder, M.T. Schuster, G. Reitz, G. Horneck, Y. Uchihori, H. Kitamura, O. Ploc, J. Kubancak, I. Nikolaev, (2015), Overview of the Liulin type instruments for space radiation measurement and their scientific results, 92–114. http://dx.doi.org/10.1016/j.lssr.2015.01.005.

Dachev, T. P., Bankov, N. G., Tomov, B. T., Matviichuk, Y. N., Dimitrov, P. G., Häder, D.-P. & Horneck, G., (2017), Overview of the ISS radiation environment observed during the ESA EXPOSE-R2 mission in 2014–2016. Space Weather, 15, 1475–1489. https://doi.org/10.1002/2016SW001580.

Friedberg, W. and Copeland, K., (2011). Ionizing Radiation in Earth's Atmosphere and in Space Near Earth, Oklahoma City, OK: Federal Aviation Administration, Civil Aerospace Medical Institute DOT Report No. DOT/FAA/AM-11/9.

Guldbakke, S., Dietz, E., Kluge, H., Schlegel, D., (1994). PTB Neutron Fields for the Calibration of Neutron Sensitive Devices, Vol. I. Physik und Messtechnik, Strahlenschutz, pp. 240–247 (Koln, Verlag TUV Rheinland).

Haffner, J. W., (1971). Yadernoe izluchenie i zashchita v kosmose (Nuclear Radiation and Protection in Space), pp 115, Atomizdat, Moscow. (book in Russian)

ICRU, (2000). Nuclear Data for Neutron and Proton Radiotherapy and for Radiation Protection, Report 63. ICRU Publication, Bethesda, MD.

McIlwain, C.E., (1961). Coordinates for mapping the distribution of magnetically trapped particles. Journal of Geophysical Research, 66,3681–3691.

Mertens, C.J., (2016). Overview of the radiation dosimetry experiment (RaD-X) flight mission. Space Weather, 14(11), 921-934.

Mertens, C.J., et al. (2016). Cosmic radiation dose measurements from the RaD-X flight campaign, Space Weather, 14, 874–898, https://doi.org/10.1002/2016SW001407.

Mitaroff, A., Silari, M., (2002). The CERN-EU high-energy reference field (CERF) facility for dosimetry at commercial flight altitudes and in space. Radiat. Prot. Dosim. 102, 7–22.

Sevast'yanov, V.D., Tarnovskii, G.B., and Lyagushin, V.I., (1997). Measurement of the Neutron Energy Spectrum on the Mir Orbital Station, Kosm. Issled., 35, 2, 216–220. [Cosmic Research, pp. 201–205].

Simpson, J. A. (1983). Composition and origin of cosmic rays. In M. M. Shapiro (Ed.), NATO ASI Series, Series C Mathematical and Physical Sciences (Vol. 107, pp. 1–24). Dordrecht: Reidel.

Smart, D.F. and Shea, M.A., (2005). A review of geomagnetic cutoff rigidities for earth-orbiting spacecraft. Advances in Space Research, 36(10), 2012-2020.

Spurný, F., (2005). Response of a Si-diode-based device to fast neutrons, Radiation Measurements, 39, 219 – 223.

Spurný, F., Ploc O., Dachev, T., (2007). On the Neutron Contribution to the Exposure Level onboard Space Vehicles, Radiation Prot. Dosimetry, 126, 519 – 523. http://rpd.oxfordjournals.org/content/126/1-4/519

Straume, T., C. J. Mertens, T. C. Lusby, B. Gersey, W. K. Tobiska, R. B. Norman, G. P. Gronoff, and A. Hands (2016), Ground-based evaluation of dosimeters for NASA high-altitude balloon flight, Space Weather, 14, https://doi.org/10.1002/2016SW001406.